EFDA–JET–PR(07)37

P.C. de Vries, M.-D. Hua, D.C. McDonald, C. Giroud, M. Janvier, M.F. Johnson,
T. Tala, K.-D Zastrow and JET EFDA contributors

Scaling of Rotation and Momentum Confinement in JET Plasmas

Scaling of Rotation and Momentum Confinement in JET Plasmas

P.C. de Vries[1], M.-D. Hua[2,3], D.C. McDonald[1], C. Giroud[1], M. Janvier[4], M.F. Johnson[1], T. Tala[5], K.-D Zastrow[1] and JET EFDA contributors*

JET-EFDA, Culham Science Centre, OX14 3DB, Abingdon, UK

[1]EURATOM/UKAEA Fusion Association, Culham Science Centre, Abingdon, OX14 3DB, UK.
[2]Imperial College, SW7 2BY, London, UK.
[3]Ecole Polytechnique, Route de Saclay, 91128, Palaiseau, France.
[4]Institute National Polytechnique de Grenoble, Grenoble, France.
[5]Association Euratom-Tekes, VTT,, P.O. Box 1000, 02044 VTT, Finland.
** See annex of M.L. Watkins et al, "Overview of JET Results ", (Proc. 21 st IAEA Fusion Energy Conference, Chengdu, China (2006)).*

Preprint of Paper to be submitted for publication in
Nuclear Fusion

ABSTRACT.
An extensive database to study the scaling of rotation and momentum transport has been constructed at JET. The database contains information from various operational scenarios, amongst them H-mode discharges, and parameters that characterise the rotation, as well as those that describe the general plasma conditions. Dimensionless Mach numbers are introduced to quantify rotation. The scaling of plasma rotation and the Mach numbers in particular has been studied. The thermal and Alfvén Mach numbers were found to scale inversely with q and with the ratio of torque and additional heating power. Although the momentum and energy confinement times were found to be of the same magnitude, the ratio was found to vary. Regression analyses showed a dependency of both the energy and momentum confinement times on plasma rotation. If rotation was included in the scaling model of energy and momentum confinement the quality of the fits substantially improved. Detailed analysis of the core and edge (pedestal) confinement showed that momentum confinement was improved in the core of the plasma compared with the energy confinement. However, the pedestal proved to be less confining for the momentum than for the energy.

1. INTRODUCTION

Rotation of Tokamak plasmas is thought to play an important role in plasma stability and the suppression of turbulence [1, 2]. It is therefore important to understand the scaling of plasma rotation and momentum confinement, in order to accurately predict ITER performance.

Previous analysis had shown a relationship between energy and momentum confinement [3, 4, 5, 6, 7]. It is often reported that these quantities have comparable magnitudes and have similar dependencies with individual plasma parameters. This is usually attributed to the coupling of heat diffusivity and viscosity. However, detailed studies have also shown cases where this relationship breaks down. In ASDEX a slightly different scaling was found for the momentum and energy confinement time, while a strong deviation was observed in discharges with peaked density profiles [8]. Similarly, a significant difference between momentum and energy confinement was found in JET discharges during ELM free phases [9]. Detailed analysis has shown that the momentum confinement time in JET plasmas does not necessarily equal the energy confinement time and that the momentum and heat diffusivities can differ significantly in the core [8]. Recent experiments at DIII-D used combined co- and counter-current NBI in order to produce plasmas with varying net torque. The experiments showed a dependency of the plasma performance with the net applied torque [10]. As plasma rotation is expected to affect turbulence, this raises the question of whether the energy and momentum confinement may depend on the rotation.

At JET a database has been created to study the general scaling of plasma rotation and momentum confinement in order to get a better understanding of the relevant parameter dependencies. The database contains information on various operational scenarios such as the ELMy H-mode baseline scenario, Hybrid and Advanced Tokamak scenarios. Usually the dominant auxiliary heating system in these JET scenarios is Neutral Beam Injection (NBI), which also supplies a considerable toroidal torque to the

plasma, hence driving large toroidal rotation. Toroidal angular rotation frequencies up to ω_ϕ = *222*krad/s have been observed in JET, which is equivalent to rotation velocities of almost *700*km/s. However, for ITER plasmas, with larger inertia and lower available NBI torque, plasma rotation is expected to be considerably lower. Therefore, a large number of discharges with dominant Ion Cyclotron Resonance Heating (ICRH), which may be representative of low torque plasmas, have also been added to the database.

Plasma rotation in JET is measured by means of Charge eXchange Recombination Spectroscopy (CXRS) [5]. It determines both the toroidal plasma rotation and ion temperature profile at *12* radial locations. The measured quantities are those of Carbon ions and in this study it is assumed that the main plasma ions have equal temperature and velocities. For H-mode plasmas this assumption generally holds. Although for plasmas with large pressure gradients, such as those with an Internal Transport Barrier (ITB), the rotation profiles may need to be corrected [12]. Typical corrections for plasmas with an internal transport barrier are $\Delta v/v_C \sim 25\text{–}35\%$, where v_C is the measured Carbon velocity. For H-mode discharges the correction never exceeds $\Delta v/v_C < 5\%$ which is within the accuracy of the diagnostic. The effect of this correction for global parameters, such as total angular momentum, which are derived from integrated or averaged profiles, is however often within the errors of these parameters. The paper will firstly describe the JET rotation database in section 2, listing the parameters and discussing the data selection and validation. Although, a large relational database has the advantage of showing overall trends and scaling, detailed variations may often be hidden by data scatter. Hence, proper data validation is required together with an understanding of the errors and parameter correlations, which will be treated in this section.

Section 3 will present the scaling of the thermal and Alfvén Mach numbers in JET plasmas. These are respectively defined as the ratio of rotation velocity and the thermal or Alfvén velocity. These are dimensionless parameters, which enable a straightforward comparison between various operational scenarios at JET or even with other devices. General profile information is also included in the database and the variation of the Mach number and toroidal rotation profiles for the different scenarios will be discussed. This section will also show the general scaling of both Mach numbers in JET.

The global momentum confinement time is discussed in section 4, where it is compared to the total energy confinement time. Furthermore, differences between confinement of momentum in the core and that by the edge pedestal will be studied. A regression analysis has been carried out to determine the principle parameter dependencies for momentum confinement. Some detailed cases will be discussed to highlight special dependencies. The results will be summarised and discussed in the final section of this paper.

2. ROTATION DATABASE AT JET

In this section the details of the JET rotation and momentum transport database will be presented. Identifying broad trends in plasma rotation and the global scaling of plasma parameters could be achieved with a relational database. The latter must include a large number of discharges from all

operation modes, with the aim of avoiding hidden correlations between parameters. Particular effort was dedicated to finding a good compromise between computing time and accuracy of the data. In addition, the database was designed to be easily generated, updated and used in any data analysis software.

2.1 DATABASE ENTRIES AND PARAMETERS

As mentioned above, the database entries include a range of operation scenarios; the baseline ELMy H-mode scenario, the advanced Tokamak scenarios with Internal Transport Barriers (ITBs) and the so-called Hybrid scenario. These database entries are a subset of dedicated databases for each of these operation scenarios, such as the main JET H-mode confinement database [13] and those for the ITB [14] and Hybrid scenario [15]. These scenarios are predominantly heated by NBI, but a selected group of discharges with a dominant fraction of ICRH has also been added. These entries are taken mainly from experiments that studied ICRH driven plasma rotation [16, 17]. Furthermore, the database contains an additional subset of JET discharges from experiments with reversed plasma current and toroidal field direction, i.e. counter-current NBI. Most of these additional entries are H-modes. Approximately, *80*% of all database entries can be described as H-mode, showing a characteristic edge pedestal and ELMs. The scenarios that appear in the rotation database are summarised in table 1, the total number of database entries for the version used in this paper (May 2007) is *574*.

All discharges are analysed in a steady-state phase. The used data is reliable in a sense that it consists of a subset of other existing databases or concerns discharges that have appeared in previous publications. To reduce parameter errors, each data signal is averaged over a *200*ms steady-state time-window. The database parameters fall into 4 categories: *general*, *energy*, *rotation* and *profile* parameters. In table 2, a summary is given of the main database parameters for each category. Note that beside global values also data describing the H-mode pedestal energy and momentum have been added, which will be analysed in section 4. In addition the database contains all information on data computation procedures, estimated error bars and possible computing errors that have occurred. When available, additional information on the background of the pulses, analysis carried out and comments of previous users is provided.

Beside the parameters mentioned in table 2, other parameters are included in the database. For instance: normalized gradient lengths of ion temperature and rotation parameters, thermal and momentum diffusivities or parameters characterising the ITB. These have been omitted in table 2, because they are not used in the analysis presented in the paper.

2.2 ERRORS, VALIDATION AND CORRELATION

In order to carry out a reliable database analysis, parameters should be validated and a proper understanding of the data errors (see table 2), and data scatter is required. Furthermore, not all parameters in the database may be entirely independent and correlations may complicate regression analysis.

The database was designed to carry out studies involving numerous discharges over several operation scenarios. To achieve this, short computing time calculations, are automatically performed using

JET's diagnostics raw signals. Some parameters, such as the normalized collisionality, cannot be reasonably computed directly. In that case, an approximated formula is used.

For each parameter of the database, a single error accounts for the uncertainty on the value of all entries. It does not take into account individual discharge conditions which might influence the data scatter. Some of the parameters can have a large uncertainty, for example the effective ion charge, Z_{eff}. It is determined from the impurity densities measured by CXRS and may be underestimated because not all impurities are included. For parameters computed from a approximated formula, the error bars are derived from benchmarks against reliable data. The parameters involving the calculation of a gradient have large error bars, of the order of *40*%. Existence diagrams of various parameters are shown in figure 1.

The size of the database implies that the accuracy of every single data point cannot be individually guaranteed. Nevertheless all orders of magnitude are checked as well as consistency with basic or well-known scalings, as for instance the correlation of torque and angular momentum (see figure 1a). The data scatter observed in this graph is expected due to differences in the momentum confinement as will be discussed later in this paper. Depending on how they were calculated, the database parameters are validated by different means. For parameters characterizing the overall discharge such as line-integrated density, the heating powers or the plasma current, a basic hand-check is done during the time-window determination. An in-depth look at all parameters for every outlier observed while using the database is also taken. As noted before, parameters computed by means of a more complex calculation, e.g. gradient computation or use of a scaling law, are benchmarked by comparison with available results from other computation methods or databases.

Contrary to the scan of a given parameter keeping all other parameters constant, the entire parameter set usually varies from one database discharge to another. Database discharges were performed over a large time span, meaning that the wall conditioning, or even the physical structure of JET, which underwent several divertor changes, could have changed. These features are sources of data scatter and may confuse the analysis.

The correlation between parameters affects the database regression analysis. In table 3 the correlations between the logarithms of a number of relevant parameters are shown. The logarithm is used here for practical reasons related to the regression analysis presented in section 3 and 4. The tables show that the magnetic field, B_ϕ, and plasma current, I_p, are not entirely independent, because of operation at distinct values of q_{95}. This is also evident from figure 1b. Similarly, in figure 1c a correlation between the total input power and the toroidal torque, T_ϕ, is found, because a major part of the database entries are predominantly NBI heated. A stronger correlation is found for the subset of H-mode discharges only as can be seen in table 3b. For the complete database, the line-integrated density, *ne*, and the NBI power, P_{NBI}, are practically uncorrelated as seen in figure 1d, although when for example only the ITB subset is considered, some correlation can be seen.

A proper analysis of trends and scaling requires a sufficient range for the involved parameters. The relevant ranges for the database parameters are given in table 2, and seem to be satisfactory. Nonetheless,

the experiments in each scenario are performed using standardized parameters and, in addition, discharges are often repeated with most of the parameters kept nominally equal. This results in these parameters being distributed in clusters, rather than in a uniform distribution. This may be detrimental to the derivation of robust scaling laws.

3. MACH NUMBER SCALING IN JET PLASMAS

The JET rotation database has been used to study the characteristics and scaling of plasma rotation, which will be presented in this section. Using dimensionless parameters is beneficial when studying the scaling of rotation, as it allows a straightforward comparison between various JET scenarios or even other devices. Previously the thermal Mach number was introduced [10], defined as the ratio of the kinetic and the thermal velocity:

$$M_{th} \equiv \frac{v_{kin}}{v_{therm}} = \sqrt{\frac{m}{e}}\,\frac{v_\phi}{\sqrt{T}} \tag{1}$$

Here, m is the mass of the species and v_ϕ its (toroidal) rotation velocity in [m/s]. The temperature, T, is given in [eV] with e the electron charge. The Mach number is the square root of the ratio of the kinetic energy and thermal energy. It depends both on the ratio of torque and heating power and the ratio of heat and momentum confinement. The Mach numbers given in this paper are for Deuterium fluid. Furthermore, one could define the Alfvén Mach number as the ratio between the plasma rotation and the Alfvén velocities:

$$M_A \equiv \frac{v_{kin}}{v_A} = \frac{v_\phi}{B_\phi / \sqrt{\mu_o \rho}} \tag{2}$$

Here, B_ϕ is the (toroidal) magnetic field strength in [T] and ρ is the mass density of the plasma species in [kg m^{-3}]. The Alfvén Mach number is related to the electromagnetic properties of the plasma and thus relevant to physics such as resistive wall mode stability [18]. In contrast the thermal Mach number is connected to instabilities or turbulences arising from fluid physics [19, 20]. It is interesting to note that the ratio of the Alfvén and thermal Mach number, as defined above, can be rewritten as:

$$\left(\frac{M_A}{M_{th}}\right)^2 = \frac{{}^1\!/_2 neT}{B_\phi{}^2 / 2\mu_0} \equiv \frac{1}{3}\,\beta_\phi \tag{3}$$

Where β_ϕ is kinetic pressure of the plasma normalised to the (toroidal) magnetic pressure. Here n is the particle density of the plasma species and T is again in [eV]. Because β_ϕ is of the order of a few percent, the Alfvén Mach number is expected to be approximately one order of magnitude smaller than the thermal Mach number. The thermal Mach number has a dependency on the temperature (see equation 1), while the Alfvén Mach number relates to the local density (or ρ in equation 2). In this section the general scaling of both these parameters will be studied and their values for various JET scenarios will be discussed.

3.1 Thermal Mach number

The relationship between the rotation and temperature profiles in predominantly NBI heated plasmas has previously been reported [6, 10]. These studies revealed an interesting trend between the central rotation velocity and ion temperature. An off-set linear scaling with the square root of the temperature is seen in figure 2a. The thermal Mach number for these points is given by the slope of a line from that point through the origin. A similar trend as shown in figure 2a is found when the total angular momentum is plotted versus the plasma kinetic energy. The Mach number may vary locally depending on the rotation and temperature profiles. A global value can be derived by means of the profile average Mach number. In figure 2b, this average thermal Mach number, $\langle M_{th} \rangle$, is plotted as a function of the ratio of toroidal torque, T_ϕ, and total auxiliary power, P_{in}. NBI is taken as the only source of toroidal torque. The average thermal Mach number is found to scale approximately with the ratio of torque to total heating power. The rotation and thermal velocity (in equation 1) are determined by the sources (torque and power) and the losses determined by the characteristics of the momentum and energy confinement. If the momentum and energy confinement are linked one would therefore expect the thermal Mach number to scale with the ratio of the sources, i.e. T_ϕ/P_{in}. Although the torque and total auxiliary power parameters in JET are correlated and hence their ratio has a restricted range, a significant scaling with the ratio of these parameters can still be observed on figure 1c. The relation between momentum and energy confinement will be discussed in detail in the next section.

For the main scenarios at JET (i.e. H-mode, Hybrid, ITB), which are often predominantly NBI heated, the average thermal Mach number is found in a range between $0.2 < \langle M_{th} \rangle < 0.5$. However, considerably lower values are found for those discharges with predominantly ICRH heating. From those discharges with a torque less than $T_\phi < 1$Nm showed thermal Mach numbers between: $0.034 < \langle M_{th} \rangle < 0.14$. The average values for each scenario are: $\langle M_{th} \rangle = 0.36 \pm 0.09$ for Type I ELMy H-mode, $\langle M_{th} \rangle = 0.25 \pm 0.07$ for Type III ELMy H-mode, $\langle M_{th} \rangle = 0.34 \pm 0.06$ for the Hybrid scenario, which feature predominantly type I ELMs, and $\langle M_{th} \rangle = 0.31 \pm 0.08$ for discharges with ITBs. The values quoted here are in each case the mean of the database subsets and its standard deviation. A significantly lower thermal Mach numbers is found for discharges with type III ELMs.

In figure 2c, the peaking factor of the thermal Mach number profile (defined as: $M_{th}(0)/\langle M_{th} \rangle$) is shown as a function of density. If peaking factor is unity the rotation profile shape equals that of the square root temperature profile. The Mach number profile is more peaked for low density, predominantly NBI heated, ITB and Hybrid, discharges, with peaking factors up to $M_{th}(0)/\langle M_{th} \rangle = 1.8$, while it is almost flat for high density H-modes. The central Mach numbers in discharges with ITBs can reach peak values up to $M_{th}(0) = 0.68$, as shown in figure 2d. The Carbon Mach numbers are a factor $\sqrt{m_c/m_D} \approx 2.4$ larger than those of the Deuterium fluid given in figure 2 and for many discharges in the database the Carbon velocity is supersonic with $M_{thC}(0) > 1$

Hollow Mach profiles, i.e $M_{th}(0)/\langle M_{th} \rangle < 1$, are found for a number of discharges in the database (see figure 2c). Either the ion temperature profile is strongly peaked while the rotation profile remains flat, or the rotation profile itself is also hollow. The majority of hollow Mach profiles are

found for discharges with dominant ICRH heating. It has been shown that ICRH could drive off-axis momentum, yielding hollow rotation profiles [16]. Furthermore, other points with $M_{th}(0)/\langle M_{th}\rangle < 1$, are found to be high density and counter-current NBI heated discharges.

3.2 ALFVÉN MACH NUMBER

The Alfvén and thermal Mach number are related according to equation 3 and their ratio is approximately $\sqrt{\beta_\phi}$. Hence, the Alfvén Mach number is an order of magnitude smaller than the thermal one. In figure 3a the squared ratio of the Alfvén and thermal Mach number is plotted against β_ϕ. The data follows the trend given by equation 3, however, the β_ϕ values are slightly larger because this data is based on the diamagnetic energy and contains a fast-particle energy component, while the vertical axis is based on thermal energy only. A number of ITB entries show a notable deviation from this trend. This may be due to an underestimation of Z_{eff} for these entries, which is used to determine the ion mass density in equation 2.

In figure 3b it can also be seen that the profile average Alfvén Mach number $\langle M_A\rangle$ scales approximately with β_ϕ. A detailed look shows that that the $\langle M_A\rangle$ is also lower for type III ELMy mode discharges compared to those with type I ELMs. Note that the higher central and average values found for ITB discharges may be overestimated as discussed above. However, as we have seen with the thermal Mach number, higher core rotation values are observed in plasmas with internal transport barriers.

The Alfvén Mach profile peaking factor is defined as $p_{MA} = M_A(0)/\langle M_A\rangle$. When the definitions of both Mach numbers are compared (see equation 1 and 2), it is clear that the Alfvén Mach number profile is expected to be more peaked than thermal Mach number profile. The M_A profile peaking is a combination of the rotation and density profile peaking. In general the profiles are more peaked for low-density discharges, as shown in figure 3c. The observed inverse trend with the density can be explained by the fact that for higher density plasmas, the torque deposition will be more off-axis, as the NBI penetration is reduced. Hence the higher density results in flatter rotation and Mach number profiles. Furthermore, the Mach profile peaking may be related to a peaking of the density profile.

In ref. [18], the relevant Alfvén Mach number, which determines stability to resistive wall modes, is not that in the centre or the average value but that at the position of an outer rational q-surface. The large peaking factor of the Alfvén Mach profile implies that the Alfvén Mach numbers at the edge are considerably lower than the values of $M_A(0)$ and $\langle M_A\rangle$ shown in figure 3b and c. Hollow Alfvén Mach number profiles are found in discharges with mainly ICRH heating or those with counter NBI, as was also found for the thermal Mach profiles for these discharges. Discharges with dominant ICRH heating featured the lowest Alfvén Mach numbers. From those discharges with a torque less than $T_\phi < 1$Nm the Alfvén Mach numbers ranged from: $0.0009 < \langle M_A\rangle < 0.008$.

3.3 DETAILED EXAMPLES

In figure 2c and 3c it can be seen that discharges that form an internal transport barrier exhibit a

peaking of the thermal and Alfvén Mach profile. In figure 4 an example is shown. The transport barrier forms at $t=5.86$s yielding an increase in central temperature but also angular rotation frequency. A strong increase of the central Alfvén Mach number, which scales with the local rotation velocity and density, occurs when the ITB forms. The central Alfvén Mach number doubles from $M_A(0)=0.03$ to 0.06. A more modest increase is seen for the thermal Mach number which nevertheless reaches a value of $M_{th}(0)=0.7$. The increases in normalisec rotation can be attributed to an improved confinement of momentum. A further observation was that type III ELMy H-mode plasmas have generally lower average Mach numbers compared to those with Type I ELMs. It has been reported previously that the transition to H-mode increases the edge thermal Mach number [10]. H-mode discharges have a flatter thermal Mach profile. In figure 5 an example is shown with a spontaneous transition from type I to III ELMs at $t=22.75$s. Both central and edge thermal Mach numbers decrease, but the edge Mach number drops more rapidly. This results in a more peaked Mach profile after the transition to type III ELMs. The average Mach number decreases. The angular momentum drops by 40% while the total energy only decreases by 13%. Because the momentum and heat sources remain constant, this indicates a change in the ratio of momentum and energy confinement times.

The formation of an H-mode pressure pedestal also affects the edge rotation. A clear example is presented in figure 6 that shows a discharge which has a marginal H-mode. Phases with good confinement and clear type I ELMs are followed by short phases, which can be characterised by a high frequency compound ELMs, and lower momentum confinement. Note that the rise in toroidal angular momentum (~28%) at each transition is more pronounced than that of the plasma energy (~19%). The central thermal and Alfvén Mach number are hardly affected whereas both edge Mach numbers increase significantly. The increase in angular momentum can be attributed to the higher edge rotation and density in this phase. During the compound phase the edge Alfvén Mach number remains at a low level ($M_A^{edge}=0.005$). But the pedestal formation shows a large rise in the edge Alfvén Mach number which can reach a value of $M_A^{edge}=0.008$ just before an ELM. This increase in M_A^{edge} is due in part to both a faster rotation velocity and an increase in edge density (see equation 2).

3.4 SCALING OF MACH NUMBERS

The average thermal and Alfvén Mach numbers, $\langle M_{th} \rangle$ and $\langle M_A \rangle$, can be used as global parameters to characterise rotation. The total angular momentum is another option, although this is not dimensionless. In figure 2 and 3, the basic trends are shown. A regression analysis was carried out for a more detailed investigation of the main parameter scaling. Besides the scaling, the analysis also indicates the coupling between the various parameters. The quality of the fit of the model to the data is given by the Pearson correlation coefficient, which is unity for a perfect fit. The normalised χ^2 which is defined as the co-variance between model and measurements, normalized to the measurement error is also an indicator to the quality of the fit.

The model that has been used provides a non-linear scaling of the Mach numbers with the main engineering parameters that define a Tokamak discharge: the line-integrated density, n_e, plasma current,

I_p, toroidal magnetic field, B_ϕ, toroidal torque, T_ϕ, and total heating power, P_{in}. The regression analysis is carried out by a linear fit to the logarithm of the non-linear model. A model with a reduced set of parameters showed a degradation of the fit result, while adding other parameters, like Z_{eff}, did not significantly improve the fit, suggesting that the above model uses the optimum parameter set. The results for $\langle M_{th} \rangle$ and $\langle M_A \rangle$ are, respectively:

$$\langle M_{th} \rangle \propto n_e^{-0.12\pm0.03} \cdot I_p^{+0.49\pm0.06} \cdot B_\phi^{-0.43\pm0.08} \cdot B_\phi^{+0.73\pm0.02} \cdot P_{in}^{-0.51\pm0.03} \quad (4)$$

$$\langle M_A \rangle \propto n_e^{-0.08\pm0.04} \cdot I_p^{+0.80\pm0.08} \cdot B_\phi^{-1.12\pm0.12} \cdot B_\phi^{+0.95\pm0.04} \cdot P_{in}^{-0.36\pm0.04} \quad (5)$$

The Pearson correlation coefficients and χ^2 for both fits (4) and (5) were found to be $\rho=0.88$, $\chi^2=1.11$ and $\rho=0.84$, $\chi^2=1.14$, respectively. The errors for each coefficient relate to the standard deviation within which the regression analysis would produce a fit of equal quality. The analysis was carried out using the complete database and the coupling between the logarithms of the parameters in this model can be found in Table 3a. As also seen from figure 1b-c, there is a degree of coupling between T_ϕ and P_{in} and I_p and B_ϕ. However, the coupling is weak enough to produce a reasonable fit to the data.

The scaling with the density is weakly negative for both the thermal and the Alfvén Mach number. A positive scaling with toroidal torque, T_ϕ, and a negative scaling with input power is found. This comes close to the basic trend shown in figure 2b for the thermal Mach number. A slightly different dependency with the ratio of torque and input power is found for the Alfvén Mach numbers. Both the thermal and Alfvén Mach numbers scale quite strongly with the inverse safety factor q_{95} (i.e. the ratio between I_p and B_ϕ), especially for the Alfvén Mach number, which scales almost linearly with the inverse q_{95}. The above shown scaling suggests that there is no plasma rotation (i.e. zero Mach numbers) when no external torque is applied. For some cases, with a limited external torque, plasma rotation was observed as shown in figure 2b. However, the regression analysis presented here is dedicated to NBI driven rotation and did not attempt to resolve the rotation driven by other means. Details about plasma rotation in JET driven without external torque can be found elsewhere [16, 17].

The thermal Mach number depends on the plasma rotation as well as ion temperature; a scaling with the total input power is therefore expected. The Alfvén Mach number is based on the plasma rotation only. It is observed usually that the energy confinement scales with the inverse input power. One may argue that a similar trend of the Alfvén Mach number scaling with the inverse input power, suggests that energy and momentum transport are related. Applying more heating power without additional torque, for example by means of ICRH, would reduce the Mach numbers. The lower Mach numbers and angular momentum can be explained by an enhanced turbulence and degradation of confinement by the additional ICRH power flux, similar as discussed in ref. [21].

A similar regression analysis can be carried out to find the scaling of the peaking factor for both the thermal and Alfvén Mach number profiles,

$$p_{Mth} \propto n_e^{-0.11\pm0.02} \cdot B_\phi^{+0.40\pm0.05} \cdot T_\phi^{+0.09\pm0.04} \cdot P_{in}^{-0.11\pm0.02} \quad (6)$$

$$p_{MA} \propto n_e^{-0.31\pm0.02} \cdot B_\phi^{+0.37\pm0.06} \cdot T_\phi^{+0.08\pm0.05} \cdot P_{in}^{-0.06\pm0.03} \quad (7)$$

Where the peaking factors are defined as $p_{M_{th}} = M_{th}(0)/\langle M_A \rangle$ and $p_{MA} = M_A(0)/\langle M_A \rangle$. The Pearson correlation coefficients and χ^2 for both fits (6) and (7) were found to be $\rho = 0.57$, $\chi^2 = 2.44$ and $\rho = 0.70$, $\chi^2 = 1.36$, respectively. It should be noted that the quality of the fit for the thermal Mach number is rather unsatisfactory. As discussed above an inverse scaling with the density is found. This matches the trends shown in figure 2c and 3c. Both peaking factors depended weakly on the ratio of torque and power.

An attempt was made to study the scaling of the dimensionless Mach numbers with other dimensionless parameters in the database, such as ρ^*, ν^* and β, but no satisfactory result was obtained. This may be due to the larger error in these parameters and the fact that these are not available for all entries in the database, limiting the data used for the regression analysis.

4. GLOBAL CONFINEMENT OF MOMENTUM

As seen in the previous section, the magnitude of plasma rotation can be characterized by the Mach numbers. Besides the source (e.g. torque) the rotation is also determined by the plasma viscosity or momentum confinement. The momentum confinement time accounts for this property of the plasma. It is defined as the ratio of the steady state total angular momentum and the torque applied to the plasma:

$$\tau_\phi \equiv \frac{L_\phi}{T_\phi} \quad (8)$$

The confinement time is, in contrast to the Mach number (profile), a global value. It is often observed that the momentum and energy confinement times of Tokamak plasmas are similar, indicating that the transport processes for energy and momentum may be linked [3, 4, 5, 6]. The steady state energy confinement time in the rotation database described here, is defined as:

$$\tau_E \equiv \frac{W_{kin}}{P_{in}} \quad (9)$$

Here, W_{kin}, is the total kinetic energy obtained by integrating the ion and electron pressure profiles. This is a different definition than the one used in the international confinement database, which subtracts the fast particle energy from the total energy to obtain the thermal energy [13]. It should be pointed out that both methods to calculate the thermal plasma energy do not always provide identical results. For a number of entries from dominant ICRH subset, the duration of NBI, necessary for the CXRS

rotation measurement, was shorter or equivalent to the energy confinement time. Hence these data have been omitted from the momentum confinement time analysis.

The momentum and energy confinement times in the database are compared in figure 7a. It shows that both parameters scale with each other, although large differences exist for individual entries. According to equation 1 it is expected that the thermal Mach number varies with the ratio of energy and momentum confinement time. In figure 7c the ratio of both confinement times is plotted versus the average thermal Mach number, showing the variation between the energy and momentum confinement times. The ratio ranges from approximately *0.8 to 1.4* for most scenarios. Less obvious is the scaling of this ratio with the average Alfvén Mach number, shown in figure 7d. Note that the data with predominant ICR heating are not following these trends.

Theory on ITG (Ion Temperature Gradient) driven turbulence predicts that the energy and momentum diffusivities are equal [22]. Recent studies at JET have shown that the energy and momentum diffusivity, at least in the plasma core, do not necessary have a one-to-one relationship [10, 19]. In figure 7b, the effective momentum and heat diffusivities differ almost by an order of magnitude. For JET the ratio of the momentum and heat diffusivity, the so-called Prandtl number, is found to be smaller than unity. These effective diffusivities are calculated via the local power and torque balance equations, as discussed in ref. [10]. The local power and torque deposition are determined from the PENCIL code [23]. It is worth mentioning that due to the inaccuracy of the ion temperature and momentum density gradients, used in the calculation, the resulting diffusivities have considerable errors (*>80*%). Nevertheless, the fact that the overall global energy and momentum confinement times are of the same order of magnitude, while the core diffusivities are not, raises the question of whether there is a distinct difference between core and edge momentum confinement.

Because plasma rotation, or more precisely the rotational shear, is thought to have a stabilising influence on plasma turbulence [2], the energy and momentum confinement times may depend on plasma rotation. Furthermore, plasma rotation may influence the H-mode pedestal stability and as a consequence the pedestal strength. Usually, these effects are difficult to disentangle in many devices due to coupling of heating source and torque. Although a coupling between these sources is evident in the JET database (see figure 1c) a possible scaling of confinement with torque may be derived from the regression results of both Mach numbers. It was seen that both Mach numbers have a slightly different scaling with T_ϕ (see equation 4 and 5. In addition, the square ratio of the Alfvén and thermal Mach number equals toroidal beta according to equation 3. Therefore the toroidal beta, and hence, the plasma energy as well as the energy confinement time, should scale with torque.

4.1 SCALING OF CONFINEMENT TIMES

In the same manner as with the Mach numbers a regression analysis was performed to study the scaling of both the momentum and energy confinement times. Studies into the scaling of the energy confinement time have been performed in great detail [13]. The resulting IPB98(y,2) scaling was derived from a fit to a large database of ELMy H-mode entries from various devices.

Using the database presented in this paper, the energy and momentum confinement time were first fitted to a model with a non-linear scaling to density, plasma current, magnetic field and input power model, while information on rotation or torque was excluded from this regression analysis. This analysis provided the following results,

$$\tau_E \propto n_e^{+0.41\pm0.02} \cdot I_p^{+0.76\pm0.08} \cdot B_\phi^{+0.26\pm0.07} \cdot P_{in}^{-0.40\pm0.02} \tag{10a}$$

$$\tau_\phi \propto n_e^{+0.47\pm0.05} \cdot I_p^{+1.14\pm0.14} \cdot B_\phi^{+0.48\pm0.14} \cdot P_{in}^{-0.54\pm0.05} \tag{10b}$$

The quality of these fits, was reasonable for the energy confinement time with $\rho = 0.78$, $\chi^2 = 1.53$. But the fit for the momentum confinement time proved unsatisfactory with $\rho = 0.63$, $\chi^2 = 8.54$. Clearly the model for the momentum confinement time missed one or more relevant parameters. The result of both fits improved when torque was introduced, yielding, $\rho = 0.80$, $\chi^2 = 1.48$ and $\rho = 0.74$, $\chi^2 = 3.96$ for the scaling of energy and momentum confinement time, respectively. The scaling of both confinement times showed very similar trends with density, plasma current, magnetic field and power. However, an inverse scaling with torque was found for the momentum confinement time while the energy confinement time scaling showed small positive scaling with torque.

The best results were, however, obtained with a model that included the average Alfvén Mach number instead of torque. This gave:

$$\tau_E \propto n_e^{+0.37\pm0.02} \cdot I_p^{+0.56\pm0.06} \cdot B_\phi^{+0.17\pm0.06} \cdot P_{in}^{-0.48\pm0.02} \cdot \langle M_A \rangle^{+0.21\pm0.02} \tag{11a}$$

$$\tau_\phi \propto n_e^{+0.39\pm0.03} \cdot I_p^{+0.79\pm0.03} \cdot B_\phi^{+0.13\pm0.11} \cdot P_{in}^{-0.75\pm0.04} \cdot \langle M_A \rangle^{+0.31\pm0.03} \tag{11b}$$

Pearson correlation coefficients and χ^2 were found to be $\rho = 0.86$, $\chi^2 = = 0.99$ and. $\rho = 0.78$, $\chi^2 = 3.7$ for the scaling of energy and momentum confinement time, respectively. Inserting the scaling for the Alfvén Mach number given by equation 5 into these scalings yields a scaling of confinement times purely based on engineering parameters, including torque. The fact that the momentum confinement time may improve with torque can also be deduced from the trend figure 1a which suggest a non-linear dependence of angular momentum with torque. The model in eq. 11 gives a vanishing energy confinement time with vanishing rotation, but one should remember that it is only valid in the operation range of JET with finite values of $\langle M_A \rangle$. Using the arbitrary parameter $1+\langle M_A \rangle$ yields a non vanishing confinement time. A fit to this model presented very similar results, with identical coefficients for the main parameters as shown in equations 11 and coefficients for the scaling with $1+\langle M_A \rangle$ of 16 ± 1 and 26 ± 2 for the energy and momentum confinement time respectively. Its validity is however also limited to JET parameter range.

It is clear, that the scaling for the energy confinement time improved when the Alfvén Mach number was used as a dependent parameter. The scaling suggests that the energy confinement would vary by approximately *19*% over the typical range of Mach numbers for typical ELMy H-mode discharges in JET ($0.24<\langle M_A \rangle<0.55$). Both confinement times show a scaling with inverse power which is characteristic for turbulent transport in Tokamak plasmas. Except for the addition of Mach number, the basic trends are similar, but not identical, to those in those in the IPB98(y,2) scaling [13]. Analysis of the database subset of H-mode only entries proved unsatisfactory, because of the strong coupling between torque and power, as shown in table 3b. However, the presence of multiple confinement modes in the database is almost certain to negatively affect the quality of the resulting fits. In particular, the use of different confinement modes to break the torque-power correlation is likely to bias the estimated exponents on these two parameters. This reduces the confidence that can be placed in the scalings of equations 10 and 11. Inclusion of data from H-mode experiments which break the torque-power correlation at JET would resolve this issue.

Hence, the exact details of the scaling coefficients should be taken with care. Furthermore, it doesn't produce information on the confinement properties for plasmas with no toroidal rotation. Nevertheless, one could conclude that for this database, rotation seems to have an influence on the confinement scaling within the JET operational range that is included in the database. Earlier observations hinted to a difference in energy and momentum confinement. The ratio of the two confinement times shows an inverse trend with $\langle M_A \rangle$ which is however weaker than that found in figure 7d.

The best fits of the energy and momentum confinement times obtained by a regression analysis of the database are shown in equations 11. Because it is rotational shear that may affect turbulence and transport a more relevant parameter would be the peaking factor of the rotation or Alfvén Mach number profile instead of the average Alfvén Mach number. It was however found that this parameter was not significant to the scaling of the total energy and confinement times. Nevertheless this parameter may have an effect on the core transport as will be discussed later in this paper.

4.2 EXAMPLES

The obtained scaling for the energy and momentum times can be highlighted by a few examples. Looking back to figure 5, in the previous section, a transition from type I to type III ELMy H-mode takes place at $t=22.75$s. This transition causes a drop of the thermal Mach number. The transition is also accompanied by a change in the ratio of plasma energy and total angular momentum, while the heating power and external torque remain constant. Clearly the ratio of energy to momentum confinement times increases. This is consistent with the scaling of this ratio with the average Mach number (as shown in figure 7c or 7d). The question remains whether the observed change in ratio is due to changes in edge characteristics, reducing the confinement of momentum during the type III phase, or caused by the slower rotation and smaller Mach number.

In figure 8 a discharge is shown where the total heating power is kept constant, while the ratio of NBI and ICRH is altered. The fraction of ICRH power to the total changes from *6*% to *44*%. The total

heating power increases slightly by *16*% from *t=13*s to *15*s. But the torque is reduced by *50*% during this phase. The plasma has type I ELMs through out this phase although the ELM frequency in the later phase is higher (an increase from *40*Hz to *90*Hz). The energy confinement time decreases from $\tau_E = 0.32$s to *0.26*s while the momentum confinement time shows a small increase from $\tau_\phi = 0.26$s to *0.28*s. During this phase, the ratio of energy and momentum confinement times increases with decreasing ratio of torque to total heating power. This is consistent with the scaling of confinement times ratio with the inverse Mach number seen before. Both examples show that although the energy and momentum confinement times have similar magnitudes, the ratio can change considerably depending on the plasma conditions.

It has previously been shown that some counter-current NBI discharges exhibit distinctly hollow Mach profiles. In figure 9 an example of such a discharge is shown. At *t = 19.5*s the already high density is further increased by gas dosing, yielding a transition from a type I to type III ELMy H-mode. The figure shows a clear collapse and complete flattening of the rotation profile, and as a result a much lower angular rotation frequency. The momentum confinement time decreases from $\tau_\phi = 0.19$s to *0.09*s after the switch on of the gas dosing. Again within a discharge the momentum confinement time changes considerably with respect to the energy confinement time. It should be noted that the counter NBI discharges also exhibit less peaked temperature profiles than those done with co-current NBI.

The torque deposition profile for co-current NBI deviates from counter-injection. In the latter case, the NBI generated ions which are trapped in banana-orbits, will have an outward radial movement, while for co-NBI this is opposite. Hence, the so-called instantaneous or $\boldsymbol{j}\times\boldsymbol{B}$ torque, will be more off-axis for counter injection [9]. This is especially evident in counter discharges with high densities, which enhance the off-axis torque deposition. The strongly off-axis torque deposition resulted in very low momentum confinement times for these discharges. TRANSP analysis showed an off-axis torque profile for this discharge, which was further enhanced during the gas-dosing phase. During the high density phase shown in figure 9, TRANSP estimated that more than *50*% of the total torque is deposited in the outer region of the plasma ($\rho > 0.7$) while for an identical co-injection case this was found to be only *20*%. However, the power deposition peaked on-axis, resulting in a peaked temperature and a flat rotation profile.

This example shows that differences in the power and torque deposition can result in different momentum and energy confinement times. The flattening of the rotation and thus Mach profiles at high density is partly revealed by the scaling in the peaking factors (equation 6 and 7). However, at present torque deposition differences between co and counter injection have not been parameterised in the database.

4.3 CORE AND PEDESTAL CONFINEMENT

The confinement times discussed above, do not distinguish between core confinement and that provided by an H-mode pedestal. The physics, that determine the gradients in both regions, differs, which may

be reflected in different scaling for the edge and core confinement. The first may be determined by turbulence driven transport while the pedestal gradient could also be limited by MHD stability [24, 25]. This can be reflected in so-called two-term or offset-linear scaling models that treat the scaling of the core and pedestal confinement independently [13, 23]. Similarly as for the plasma energy, this can be used to study the difference between core and pedestal momentum confinement. As has been mentioned above, there are indications that the pedestal confinement for momentum and energy may differ.

The database contains information on the edge or pedestal energy, W^{ped}, and the so-called pedestal momentum, L_ϕ^{ped}. These quantities are determined for each entry (even those without a clear H-mode pedestal) by taking the measurement of the kinetic pressure and momentum density at the edge of the plasma ($r/a=0.89$) multiplied with the plasma volume (because the volume contained by this region is in fact slightly smaller it is actually multiplied with *95*% of the volume). The fixed position is chosen in order to simplify the calculation of these parameters for all database entries. It coincides with a major radius of approximately $R\sim3.8$m, which is close to the location of the outer most reliable ion temperature measurement. The width of the H-mode pedestal is not known for most of the database entries. Another issue is the time resolution of the CXRS diagnostic that measures the rotation and ion temperature. The edge parameters L_ϕ^{ped} and W^{ped} are averaged over period that could experience several ELM pedestal collapses. All these uncertainties make that the percentage error for the pedestal parameters higher than those of the total integrated energy and angular moment (see table 2).
In figure 10a the pedestal momentum is found to follow pedestal energy. The highest pedestal values are of course found for the H-mode entries. A simple fit to the data gives,

$$L^{ped} = 0.69 \pm 0.08.W^{ped+1.1\pm0.1} \tag{12}$$

With a Pearson correlation coefficient of $\rho = 0.82$, with L^{ped} in [kg m^2 s^{-2}] and W^{ped} in [MJ]. The fraction of energy in the pedestal almost always exceeds that of the fraction of momentum in the pedestal. This is especially true for the type I ELMy H-mode discharges. For these H-mode entries the average pedestal energy fraction is of the order of *60*% while the fraction of the pedestal to the total momentum confinement is approximately *40*%. Notably quite a number of counter discharges do not follow this trend.

The energy and momentum stored in the core, W^{core} and L_ϕ^{core}, respectively, are found by subtracting the pedestal values from the total, W^{kin} and L_ϕ. The two-term energy and momentum confinement time separating the core and pedestal physics can be defined as,
kin core ped

$$\tau_E = \frac{W^{kin}}{P_{in}} = \frac{W^{core} + W^{ped}}{P_{in}} = \tau_E^{core} + \tau_E^{ped} \tag{13}$$

$$\tau_\phi = \frac{L_\phi}{T_\phi} = \frac{L_\phi^{core} + L_\phi^{ped}}{T_\phi} = \tau_\phi^{core} + \tau_\phi^{ped} \tag{14}$$

The comparison of these parameters provides interesting information about the differences between the confinement of energy and momentum in the core and edge or pedestal region. For most of the predominantly NBI heated H-mode entries the ratio of torque and input power is of the order of $T_\phi/P_{in} \approx 1.1 \pm 0.15$ [Nm/MW]. With this information equation 12 therefore indicates that the pedestal confinement of momentum is lower than that for the energy. It should be noted that a split between the core and pedestal momentum confinement times is only possible in the case the plasma rotation is uni-directional, which is the case for standard JET operations (see figure 10a).

In figure 10b and 10c the momentum and energy confinement times for the edge (pedestal) and core are compared, respectively. Figure 10c shows, that the edge momentum confinement time is significantly smaller than that of the energy. The H-mode pedestal mainly improves the energy confinement. The reverse is found in the core, quite a large number of, mainly H-mode entries show a larger confinement for momentum than energy in the core. This is consistent with earlier observations that in JET the effective momentum diffusivity in the core is smaller than that for the ion heat diffusivity [10]. The small Prandtl numbers found in JET are due to a combination of a difference in core momentum and energy confinement times, as well as larger gradient lengths for the ion temperature profile compared to that of the momentum density. The total confinement times for momentum and energy may still have similar magnitudes, like seen in figure 7a, as the differences in core and edge confinement seem to compensate each other.

In the example in figure 9 it turns out that it is the core momentum confinement time that is degraded while the edge/pedestal confinement stays largely unchanged by the increased density. In figure 7c and 7d it was shown that the momentum and energy confinement time differ due to variations in the rotation itself. It turns out that this effect is due to core physics as it is the ratio of core momentum and energy confinement times that is changed by Mach number, as shown in figure 10d, while the edge confinement times were found to be unaffected. Figure 10d shows that the ratio of core energy and momentum confinement time is often smaller than unity (i.e. momentum confinement is better) and that this ratio decreases for larger thermal Mach numbers. It was recently shown that the presence of a momentum pinch could reduce the effective momentum diffusivity in the plasma core, hence increasing the core momentum confinement time with respect to that of the energy [26]. The observed trend in figure 10d is in agreement the studies shown in refs. [19, 26, 27] which predict a smaller effective momentum diffusivity for larger Mach numbers due to the presence of an inward pinch.

Changes in the pedestal confinement of momentum are also responsible for the differences observed between type I ELMy H-mode discharges and those with type III or compound ELMs as shown in figure 5 and 6. The transition from type I to type III ELMs shown in figure 5, causes a *40*% reduction in the pedestal momentum confinement (from $\tau_\phi^{ped} = 0.083$s to $\tau_\phi^{ped} = 0.049$s) while the core momentum confinement time remains unchanged at $\tau_\phi^{core} = 0.036$s. The transition causes only a *12*% reduction in energy confinement (τ_ϕ^{kin}=0.18s to τ_ϕ^{kin}=*0.16*s). Similarly, the compound phases in figure 6 are characterised by a low pedestal momentum confinement time, while the core momentum confinement is more or less unchanged over these transitions.

DISCUSSION

A large steady-state rotation database including all plasma scenarios, a compromise between parameter accuracy and large number of entries, has been built at JET. This database proved efficient in identifying broad trends in plasma behaviour as concerns rotation, although its quality is still affected by problems inherent to large databases, such as correlations or clusters in parameter space. This paper reported on observed trends found with this database and gave an overview of the general characteristics of toroidal plasma rotation in JET.

An offset scaling of central velocity with central ion temperature was found, with a similar trend for the global values total angular momentum and kinetic energy. Profile average thermal Mach numbers of about $M_{th} = 0.33$ are observed on JET, roughly scaling with total power divided by torque. The Alfvén Mach number is one order of magnitude lower and is observed to scale with β_ϕ. Type I ELMy H-modes have the highest values, whereas both Mach numbers in Type III ELMy H-modes are significantly lower. M_A values are higher in ITB discharges than other scenarios, while this is not observed for M_{th}. Both Mach numbers profiles are less peaked in high-density discharges and can become hollow for predominantly ICRH-heated and counter-NBI shots. For those discharges with minimum external torque ($T_\phi < 1$Nm) the Alfvén Mach numbers ranged from: $0.0009 < \langle M_A \rangle < 0.008$. The question is how these values relate to the intrinsic rotation that is observed in other devices [26].

Regression analyses were carried out on both Mach numbers. The best fit to the data was found using Tokamak engineering parameters. They showed a negative scaling with line-averaged density, toroidal magnetic field and torque and a positive scaling with plasma current and total power. The Mach profile shape depends strongly on the density, as more torque is deposited off-axis for high density JET discharges. As concerns transport, the energy and momentum confinement times were found to be approximately equal. The τ_ϕ/τ_E ratio scales with the thermal Mach number, as expected by definitions of these parameters. This ratio also scales with the Alfvén Mach number, although this parameter does not include energy or power, hinting to a role of rotation in confinement properties.

Coupling exists between various parameters, such as torque and power, which complicated the regression analysis. A principle component analysis, similar to that discussed in ref. [13], was carried out which indicating that the database had only 3 well conditioned components. If the subset of H-mode only entries are considered the coupling between torque and power further reduces the number of principle components to 2. This shows that the database presented in this paper is less well defined than the energy confinement database use to determine the H98(y,2) scaling which has 5 well conditioned principle components [13]. Therefore, the predictive power of these scaling laws is limited although they show trends within the JET parameter range. A better understanding of these scaling of rotation and momentum confinement, especially for the H-mode subset, would require further experiments designed so as to break the correlation between power and torque, for example by increasing the fraction of ICRH power in JET plasmas.

Distinction of the core and pedestal contributions to the energy and momentum revealed the difference in confinement of these regions. An H-mode pedestal leads to a larger increase in W^{ped} than

L_ϕ^{ped}, whereas the core values remain unaffected. This is consistent with the difference in average Mach numbers in Type I and III ELMy H-modes, which is predominantly caused by edge differences. The edge momentum confinement time improves less than the edge energy confinement time in the presence of an H-mode pedestal. The pedestal energy and momentum confinement are clearly governed by different physics, where the pedestal viscosity may possibly be influenced by edge radial electric fields, error fields, interaction with neutrals etc., effects that do not play a role in the energy pedestal.

The ratio of the core energy and core momentum confinement times scales with the Mach number. It has been shown that the effective momentum diffusivity is lower than the heat diffusivity in the core which leads to a larger core momentum confinement time compared to that of the energy. It was recently shown that an inward momentum pinch could explain the improved core momentum confinement [27, 28]. Experimental indications of such a momentum pinch were found at JET [19]. The better momentum confinement in the core balances the lower edge momentum confinement, which explains why the ratio of total energy and momentum confinement time has approximately the same magnitude. Studies into the difference between core and pedestal momentum confinement would benefit from experiments in which these parameters can be determined with a better accuracy.

A number of counter current NBI discharges were found to deviate from other entries. It was already pointed out, that these discharges often exhibit hollow Mach profiles. These emphasized the importance of profile effects. Generally, discharges with counter current NBI exhibited a smaller angular momentum than those with similar toroidal torque but co-NBI. However, the database was not equipped with sufficient information to distinguish trends related to differences in torque and power deposition. This urges to include more detailed profile information for further transport studies.

The JET rotation database enables the identification of the role played by rotation in confinement. Nonetheless, these results are to be considered carefully. Rotation can differ from device to device due to differences in heating systems, error fields, Toroidal Field ripple or edge viscosity driven by neutrals. It has been shown that TF ripple can have a profound influence on plasma rotation [29, 30]. Of particular importance is the orientation of NBI, ranging from normal to tangential, and their direction relative to the plasma current, counter or co-injection. Recent experiments at DIII-D showed that with balanced NBI operation and zero torque input, the plasma may still have a significant rotation [31]. The presence of an intrinsic momentum source is important for momentum transport studies where a proper understanding of the source is significant. This database is limited to a single machine, meaning a restricted region in parameter space. The scaling laws derived by regression are valid only in the vicinity of this region.

With a larger moment of inertia but a torque only twice as high than JET, it is expected that ITER will rotate slower, i.e. smaller average Mach numbers. The higher fraction of ICRH may result in hollow Mach profiles. Off-axis torque deposition may enhance this effect. The Toroidal Field ripple will also be considerably higher in ITER compared to JET [29]. All these factors make it difficult to extrapolate the experimental results presented in this paper to ITER. An extension of the database with data from other devices would be beneficial to enable confident ITER extrapolations.

ACKNOWLEDGEMENTS

The authors would like to acknowledge A. Thyagaraja for his support and help with the understanding of plasma rotation. Alfonso Baciero is thanked for his work on the profile fitting routine. This research has been performed under the European Fusion Development Agreement and was partly funded by the UKAEA, the UK Engineering and Physical Sciences Research Council, the Ecole Polytechnique (Palaiseau), the British Council and by the European Communities under contract of association between EURATOM and UKAEA. The views and opinions expressed herein do not necessarily reflect those of the European Commission.

REFERENCES

[1]. A.M. Garofalo, *et al. Nucl. Fusion* **41** (2001) 1171.
[2]. K.H. Burell, *Phys. Plasmas* **4** (1997) 1499.
[3]. S. Suckewer, *et al., Nucl. Fusion* **21** (1981) 1301.
[4]. R.C. Isler, *et al., Nucl. Fusion* **26** (1986) 391.
[5]. H. Weisen, *et al., Nucl. Fusion* **29** (1989) 2187.
[6]. J.S. deGrassie, *et al., Nucl. Fusion* **43** (2003) 142.
[7]. Y. Miura, *et al., Plasma Phys. Control. Fusion* **40** (1998) 799.
[8]. A. Kallenbach, *et al., Plasma Phys. Control. Fusion* **33** (1991) 595.
[9]. K.-D. Zastrow, *et al., Nucl. Fusion* **38** (1998) 257.
[10]. P.C. de Vries, *et al., Plasma Phys. Control. Fusion* **48** (2006) 1693.
[11]. T.C. Luce, *et al.*, in Fusion Energy 2006 (Proc. 21st Int. Conf. Chengdu, 2006) (Vienna: IAEA) CD-ROM file PD-3.
[12]. D. Testa, *et al., Phys. Plasmas* **9** (2002) 243.
[13]. D.C. McDonald, *et al., Nucl. Fusion* **47** (2007) 147.
[14]. E. Joffrin, *et al., Nucl. Fusion* **45** (2005) 626.
[15]. A.C.C. Sips, *et al., Plasma Phys. Control. Fusion* **44** (2002) A391.
[16]. L.-G. Eriksson, *et al., Phys. Rev. Letters* **92** (2004) 235001-1/4.
[17]. J.-M. Noterdaeme, *et al., Nucl. Fusio*n **43** (2003) 274.
[18]. H. Reimerdes, *et al.*, Proc. of the 32th EPS Conf. Plasma Phys., Tarragona, 2005, ECA Vol. 3 **29C** (2005) p5-056.
[19]. T. Tala, *et al., Plasma Phys. Control. Fusion* **49** (2007) B291.
[20]. A. Thyagaraja, private communication.
[21]. D. Nishijima, *et al., Plasma Phys. Control. Fusion* **47** (2005) 89.
[22]. N. Mattor and P. Diamond, *Phys. Fluids* **31** (1998) 1180.
[23]. C.D. Challis, *et al., Nucl. Fusion* **29**(1989) 563.
[24]. T. Takizuka, *Plasma Phys. Control. Fusion* **40** (1998) 851.
[25]. G. Cordey, *Nucl. Fusion* **43** (2003) 670.
[26]. J.E. Rice, *et al., Nucl. Fusion* **47** (2007) 1618.

[27]. A.G. Peeters, *et al.*, *Phys. Rev. Lett.* **98** (2007) 265003.
[28]. A.G. Peeters and C. Angioni, *Phys. Plasmas* **12** (2005) 072515.
[29]. P.C. de Vries, *et al.*, '*The Effect of Toroidal Field Ripple on Plasma Rotation in JET*', in the Proc. of 34th EPS Conf. on Plasma Phys. Control. Fusion (Warsaw, 2007).
[30]. H. Urano, *et al.*, *Nucl. Fusion* **47** (2007) 706.
[31]. W.M. Solomon, *et al.*, *Plasma Phys. Control. Fusion* **49** (2007) B313.

JET scenario	Entries	Symbol	Connecting database
ELMy H-mode	239 + 60	● + ○	H-mode confinement database [13]
Counter NBI	37	◇	
Dominant ICRH	65	□	
Hybrid	110	△	Hybrid database [15]
ITB	63	▲	ITB database [14]
Total	**574**		

Table 1: A summary of the operation scenarios and total number of entries, as for April 2007, in the JET rotation database. Part of the database has overlap with other experimental databases as indicated in the last column. The symbols will be used in this report to distinguish the operational scenarios. The closed and open circles are used for Type I and Type IIII ELMy H-mode, respectively.

Category	Name	Symbol	Unit	Range	Error
General	Electron line-integrated density	n_e	10^{19} m^{-2}	*3.90 - 28.2*	*1%*
	Toroidal magnetic field	B	T	*0.99 - 3.56*	*2%*
	Plasma current	I_p	MA	*0.98 - 3.99*	*3%*
	Toroidal β (Normalised pressure)	β_ϕ	%	*0.17 - 3.00*	*5%*
	Normalised β	β_N		*0.32 - 2.99*	*5%*
	Normalised collisionnality	ν^*			...
	Normalised Larmor Radius	ρ^*			...
	Ion effective charge	Z_{eff}	e	*1.00 - 4.20*	...
Energy	NBI input power	P_{NBI}	MW	*1.85 - 21.0*	*2%*
	ICRH input power	P_{ICRH}	MW	*0.0 - 7.45*	*2%*
	LHCD input power	P_{LHCD}	MW	*0.0 - 2.85*	*5%*
	Central ion temperature	$T_i(0)$	keV		*5%*
	Central electron temperature	$T_e(0)$	keV		*10%*
	Diamagnetic energy	W_{dia}	MJ	*0.68 - 12.2*	*5%*
	Total kinetic energy	W_{kin}	MJ	*0.51 - 9.09*	*5%*
	Pedestal kinetic energy	W_{ped}	MJ	*0.22-5.64*	*10%*
	Total energy confinement time	τ_E	s		*5%*
	Pedestal energy confinement time	τ_E^{ped}	s		*15%*
	Kinetic energy confinement time	τ_{Ekin}	s	*0.067-0.493*	*8 %*
Rotation	Central angular frequency	$\omega(0)$	krad.s^{-1}	*2.46 - 222*	*10%*
	Central ion toroidal velocity	$v_\phi(0)$	km.s^{-1}	*8.72 - 687*	*5%*
	Maximal ion toroidal velocity	$v_{\phi max}$	km.s^{-1}	*8.72 - 706*	*5%*
	Total toroidal angular momentum	L_ϕ	kg. m^2.s^{-1}	*0.04 - 9.04*	*10%*
	Pedestal toroidal angular momentum	L_ϕ^{ped}	kg. m^2.s^{-1}	*0.056-4.21*	*1 5%*
	Toroidal torque (by NBI)	T_ϕ	N.m	*0.31 - 23.1*	*2%*
	Total momentum confinement time	τ_ϕ	s	*0.049-0.585*	*8 %*
	Pedestal mom. confinement time	τ_ϕ^{ped}	s		*15%*
	Central thermal Mach number	M_{th}		*0.03 - 0.76*	*16%*
	Averaged thermal Mach number	$\langle M_{th} \rangle$		*0.02 - 0.62*	*5%*
	Central Alfvén Mach number	$M_A(0)$		*0.001 - 0.05*	*20%*
	Averaged Alfvén Mach number	$\langle M_A \rangle$		*0.0009 - 0.07*	*6%*
Profile	Thermal Mach number peaking factor	p_{Mth}			*17%*
	Alfvén Mach number peaking factor	p_{Ma}			*21%*
	....				
	....				

Table 2: An Overview of the main database parameters. For several parameters the range and an indication of the approximate error are given.

a	ln n_e	ln I_p	ln B_ϕ	ln P_{tot}	ln T_ϕ	ln $\langle M_A \rangle$
ln n_e	+1.000	+0.423	+0.116	+0.437	+0.493	+0.426
ln I_p	+0.423	+1.000	**+0.749**	+0.372	+0.209	+0.073
ln B_ϕ	+0.116	**+0.749**	+1.000	+0.362	+0.100	-0.199
ln P_{tot}	+0.437	+0.372	+0.362	+1.000	**+0.799**	+0.528
ln T_ϕ	+0.493	+0.209	+0.100	**+0.799**	+1.000	**+0.817**
ln $\langle M_A \rangle$	+0.426	+0.073	-0.199	+0.528	**+0.817**	+1.000

b	ln n_e	ln I_p	ln B_ϕ	ln P_{tot}	ln T_ϕ	ln $\langle M_A \rangle$
ln n_e	+1.000	+0.682	+0.486	+0.376	+0.407	+0.188
ln I_p	+0.682	+1.000	**+0.802**	+0.451	+0.373	-0.049
ln B_ϕ	+0.486	**+0.802**	+1.000	+0.584	+0.486	-0.229
ln P_{tot}	+0.376	+0.451	+0.584	+1.000	**+0.925**	+0.203
ln T_ϕ	+0.407	+0.373	+0.486	**+0.925**	+1.000	**+0.824**
ln $\langle M_A \rangle$	+0.188	-0.049	-0.229	+0.203	**+0.824**	+1.000

Table 3: a) Correlation matrix for the natural logarithm for a number of parameters obtained using the complete database. b) Correlation matrix for the natural logarithm of various parameters in a subset of the database containing H-mode only (i.e. Type I, III EMLy H-mode and Hybrid scenarios). Zero indicates no correlation while unity means a one-to-one relationship between these parameters. The strongest correlations (>0.7*) are shown in bold face.*

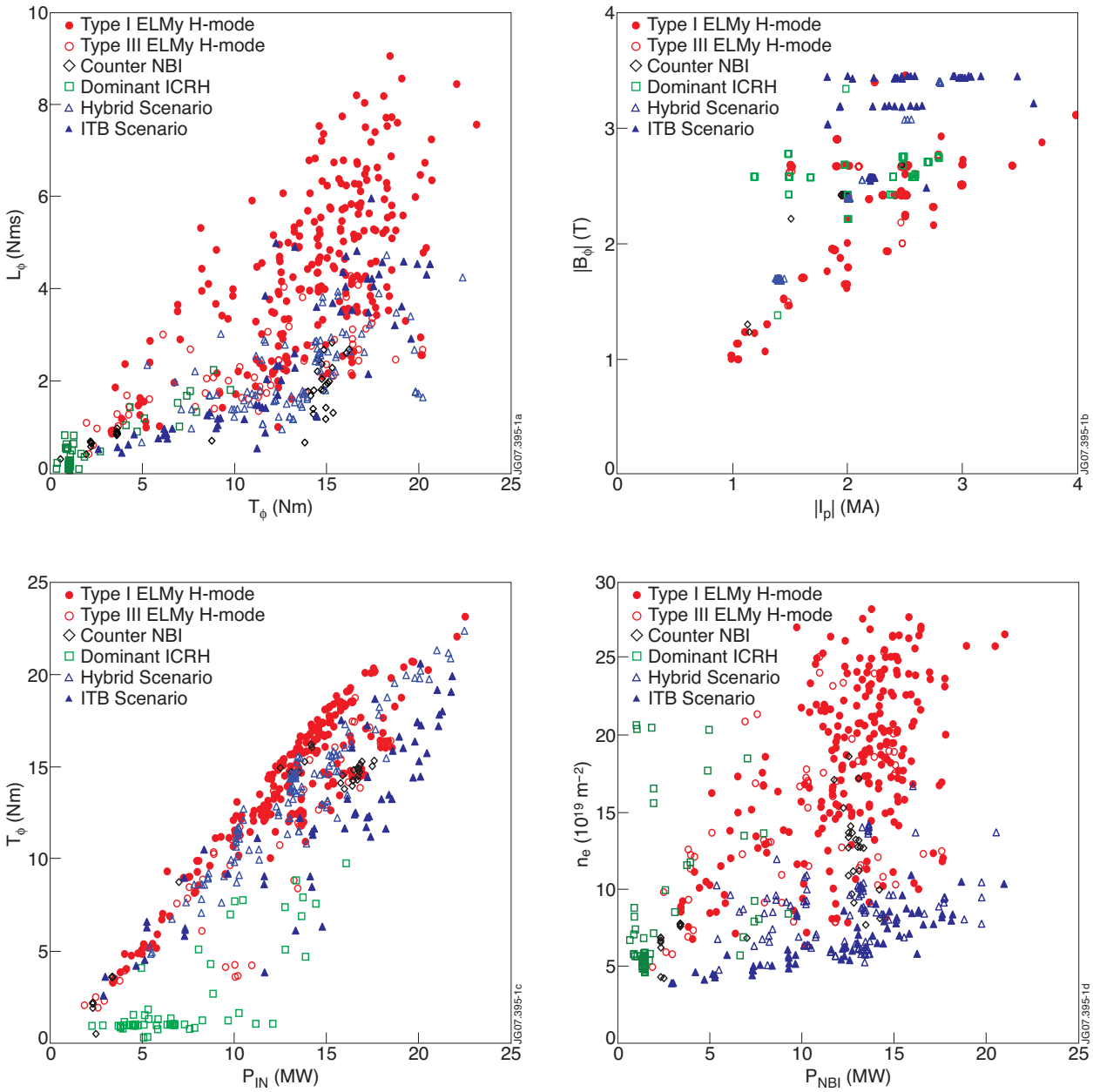

Figure 1: a) The total toroidal angular momentum as a function of the total toroidal torque for various scenarios. b) The toroidal central magnetic field as a function of the plasma current. c) The total toroidal torque as a function of the total input power. d) The line integrated electron density as a function of the NBI power input.

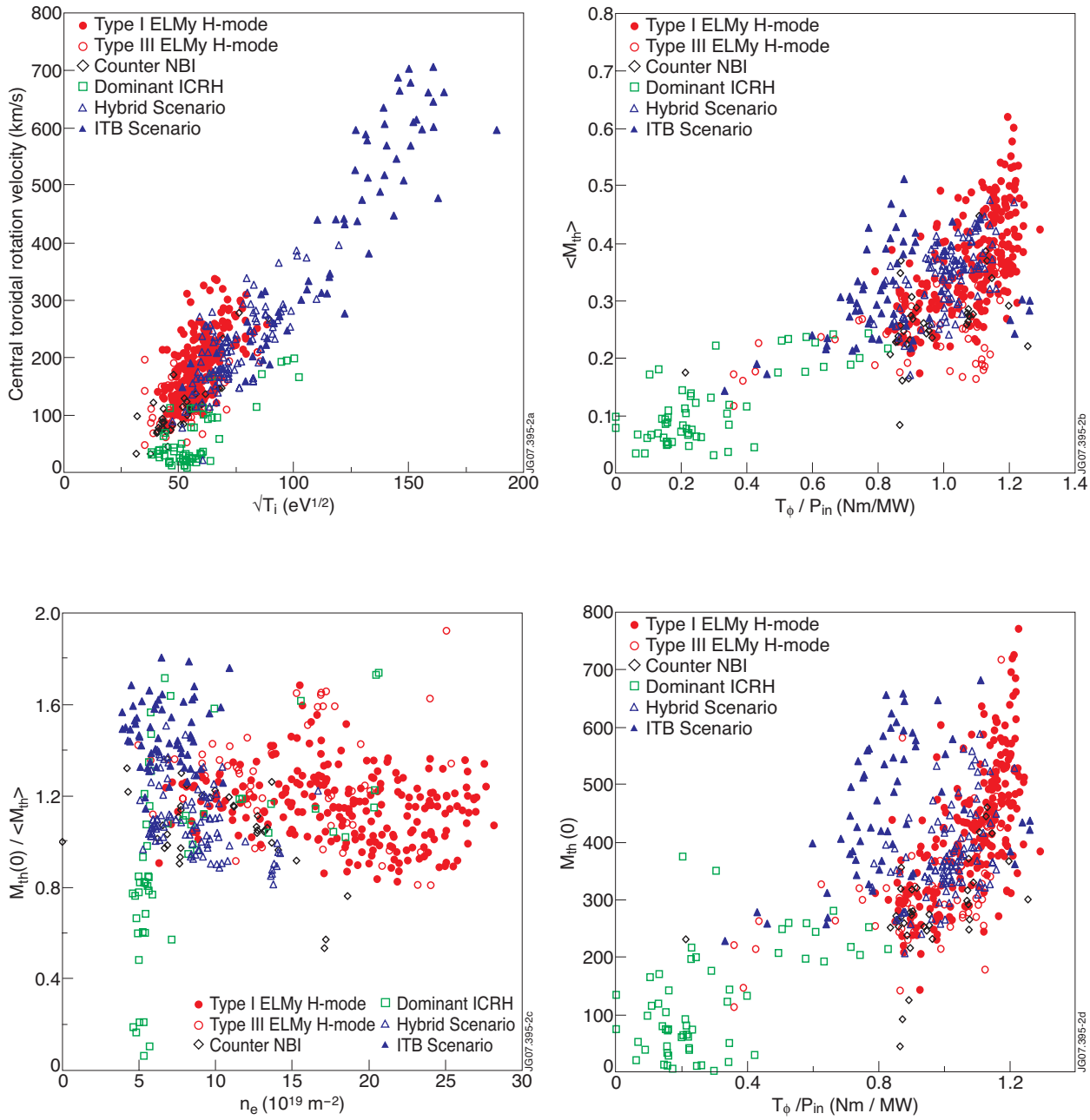

Figure 2: a) The central toroidal rotation velocity as a function of the square root of the temperature at the same location, for various scenarios. b) The profile averaged thermal Mach number, $\langle M_{th} \rangle$, as a function of the ratio of toroidal torque, T_ϕ, and total auxiliary power, P_{tot}. c) The peaking factor of the thermal Mach profile, $M_{th}(0)/\langle M_{th} \rangle$, as a function of the line averaged density. d) The thermal Mach number in the centre of the plasma, $M_{th}(0)$ as a function of the ratio of toroidal torque, T_ϕ, and total auxiliary power, P_{tot}.

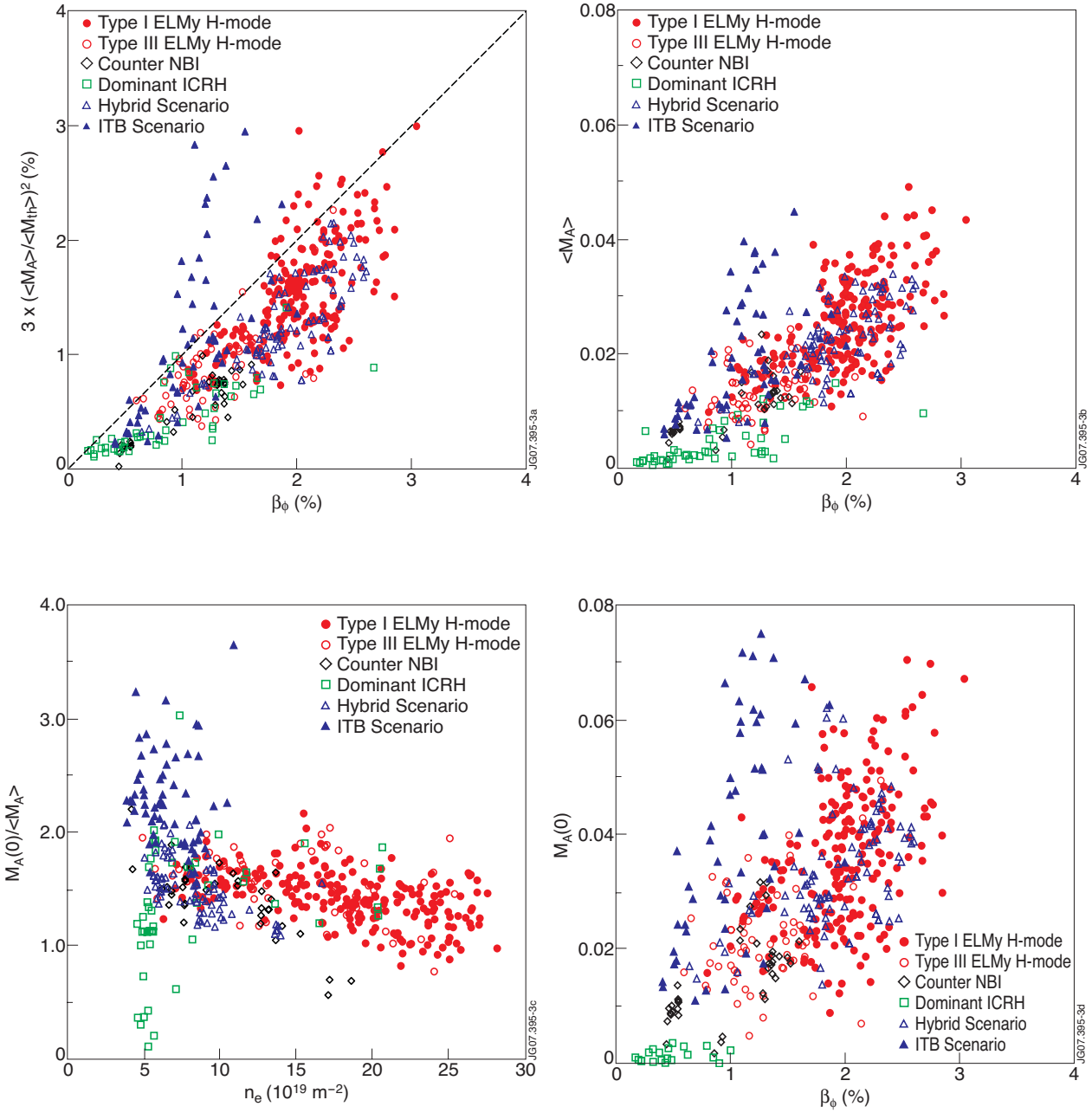

Figure 3: a) The squared ratio of the Alfvén and thermal Mach number plotted versus β_ϕ. b) The profile averaged Alfvén Mach number, $\langle M_{th} \rangle$, as a function of β_ϕ. c) The peaking factor of the Alfvén Mach profile, $M_A(0)/\langle M_A \rangle$ as a function of the line averaged density. d) The Alfvén Mach number in the centre of the plasma, $M_A(0)$.

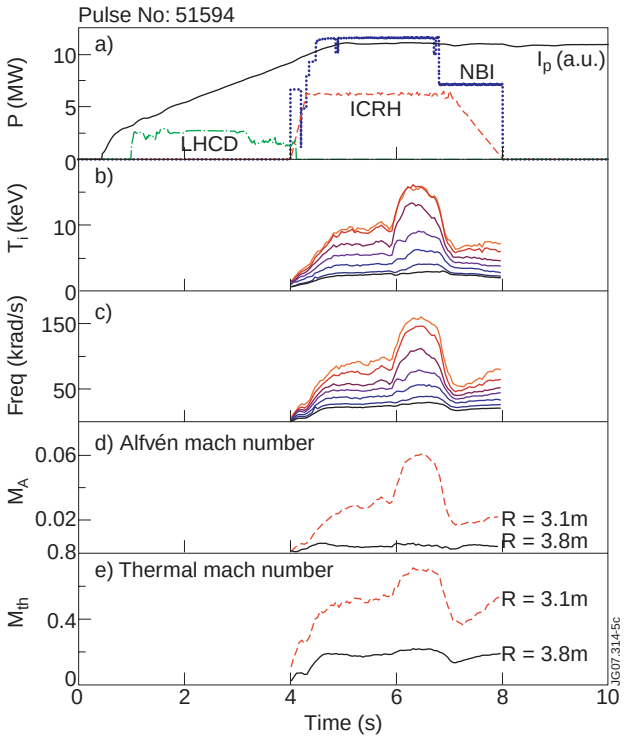

Figure 4: Example of a JET Pulse No: (51594) that forms an internal transport barrier at t=5.86s. a) Shows a typical optimised shear discharge sequence, with LHCD heating (green) during the current ramp phase, and a start of the main heating (NBI (blue dotted) and ICRH (red dashed) just prior to the start of the flat-top. b) and c) show the ion temperature and angular rotation frequency, respectively, at various radial positions. d) The Alfvén Mach number in the core (R=3.10m, red dashed) and at the edge (R=3.77m, black solid). e) The thermal Mach number in the core (R=3.10m, red dashed) and at the edge (R=3.77m, black solid).

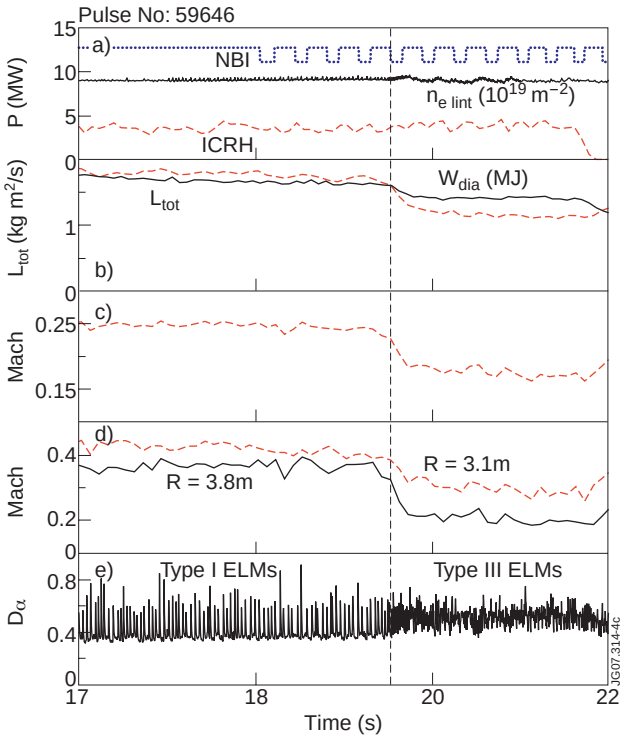

Figure 5: Example of a JET Pulse No: (59646) with a spontaneous transition from type I to III ELMs at t=22.75s, indicated by the dashed vertical line. a) The top box shows the constant input powers of NBI (blue dotted) and ICRH (red dashed) and the line-integrated density (black solid) b) The traces of the total angular momentum (red dashed) and the diamagnetic energy (black solid). c) The average thermal Mach number. d) The centre (R=3.1m)(red dashed) and edge (R=3.77m)(black solid) thermal Mach number. e) The D_α trace, indicating the ELM type.

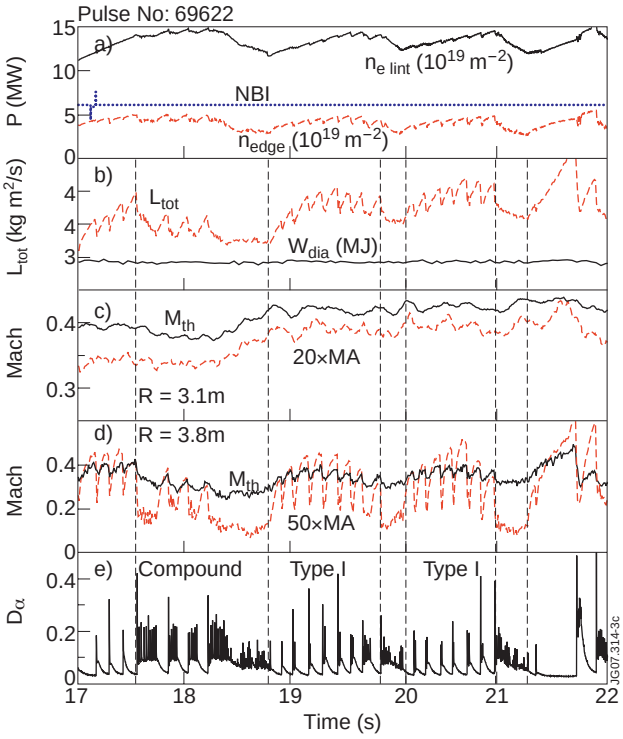

Figure 6: Example of a JET Pulse No: (69622) with a marginal H-mode resulting in phases with good type I and higher frequency compound ELMs separated by the dashed vertical lines. a) The top box shows the constant NBI powers (blue dotted) and the core (black solid) and edge (red dashed) line-integrated density. b) The traces of the total angular momentum (red dashed) and the diamagnetic energy (black solid). c) The thermal (red dashed) and Alfvén (black solid) Mach number in the centre (R=3.1m). d) The thermal (red dashed) and Alfvén (black soldid) Mach number at the edge (R=3.77m). The central and edge Alfvén Mach numbers have been scaled with factors 20 and 50, respectively. e) The D_α trace, indicating the ELM type.

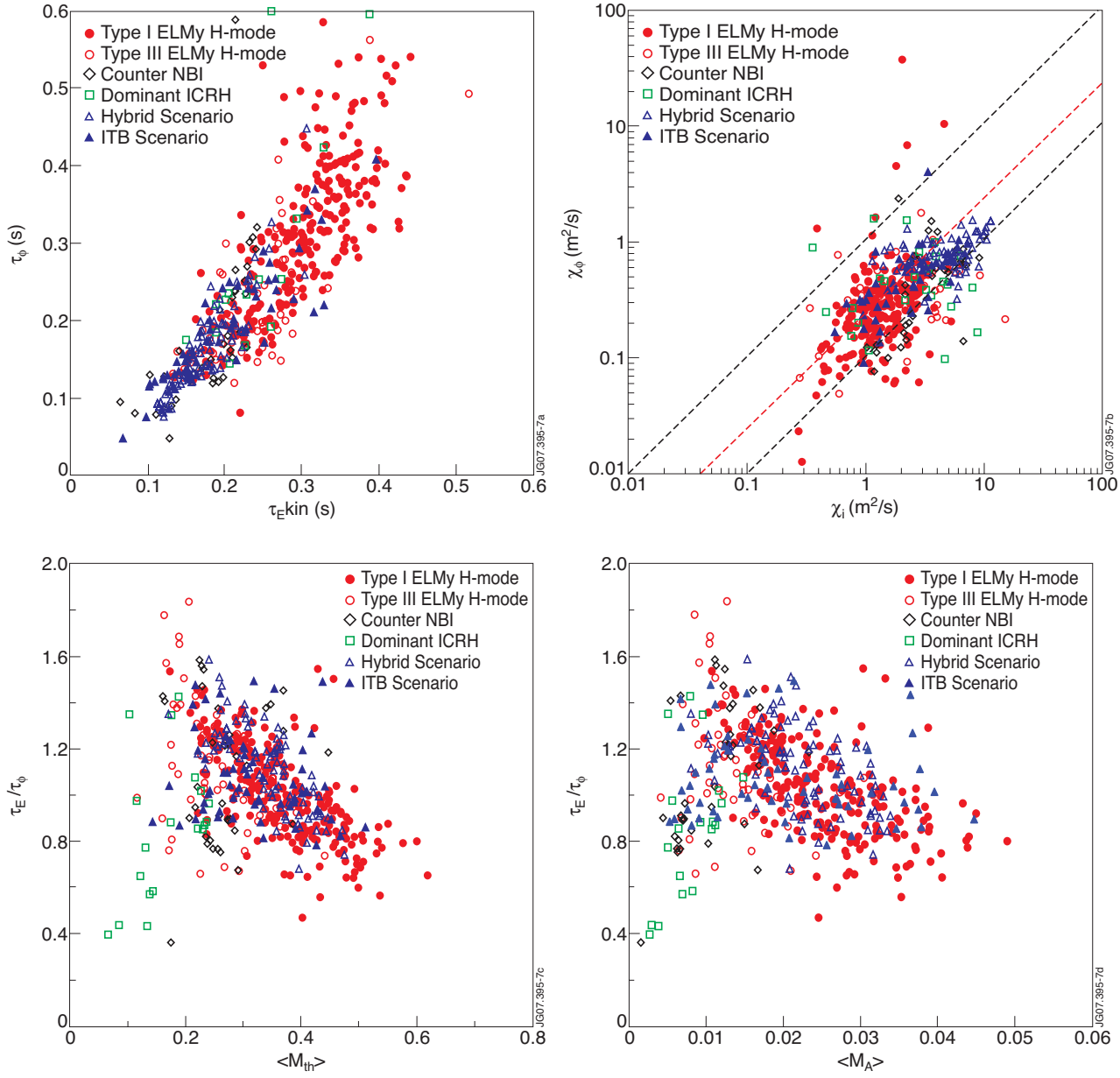

Figure 7: a) The momentum confinement time, τ_ϕ, versus the kinetic energy confinement time, τ_E. b) The effective momentum diffusivity, χ_ϕ, versus the ion heat diffusivity, χ_i, calculated via the local torque and power balance, respectively, for all entries in the database. The local power and torque deposition are determined from the PENCIL code [23]. The data is averaged from r/a=0.2 to r/a=0.7. c) The ratio of energy and momentum confinement times versus the average thermal Mach number, $\langle M_{th} \rangle$. d) The ratio of energy and momentum confinement times versus the average Alfvén Mach number, $\langle M_A \rangle$.

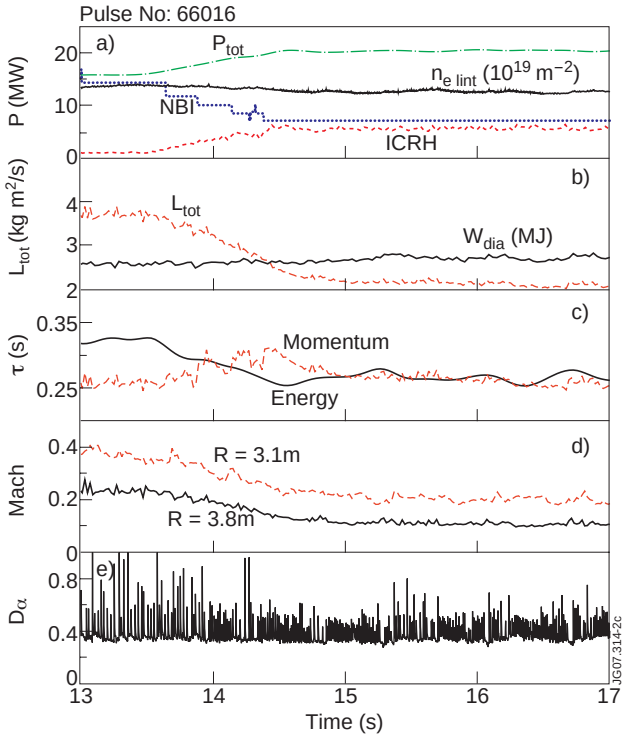

Figure 8: Example of a JET Pulse No: (66016) in which the total heating power is kept almost, while the fraction of ICRH and NBI is altered. The fraction of ICRH power to the total changes from 6% to 44%. a) The top box shows the powers of NBI (blue dotted), ICRH (red dashed) and total power (green dot-dashed) and the line-integrated density (black solid) which remained constant b) The traces of the total angular momentum (red dashed) and the diamagnetic energy (black solid). c) The energy (black solid) and momentum (red dashed) confinement times. d) The centre (R=3.1m)(red dashed) and edge (R=3.77m)(black solid) thermal Mach number. e) The D_α trace, indicating the ELM type.

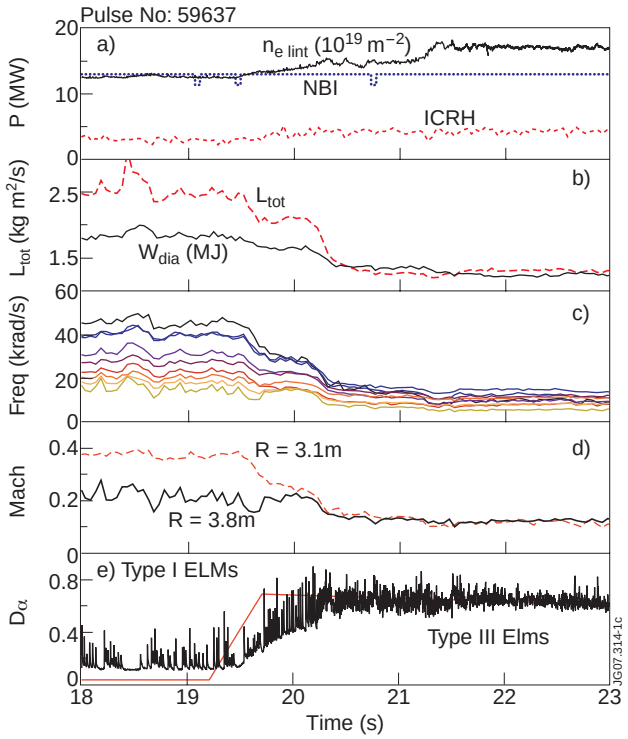

Figure 9: Example of a JET Pulse No: (59637) with counter NBI injection. Gas dosing is applied after t=19.5s, yielding a transition from type I to typ III ELMy H-mode. Although this results in only a small increase in line-averaged density, the rotation profile collapses and flattens. a) he top box shows the powers of NBI (blue dotted), ICRH (red dashed) and the line-integrated density (black solid) b) The traces of the total angular momentum (red dashed) and the diamagnetic energy (black solid). c) Angular rotation frequency at 9 radial locations (from centre to edge) d) The edge (black solid) and core (red dashed) thermal Mach number. e) The D_α trace, indicating the ELM type.

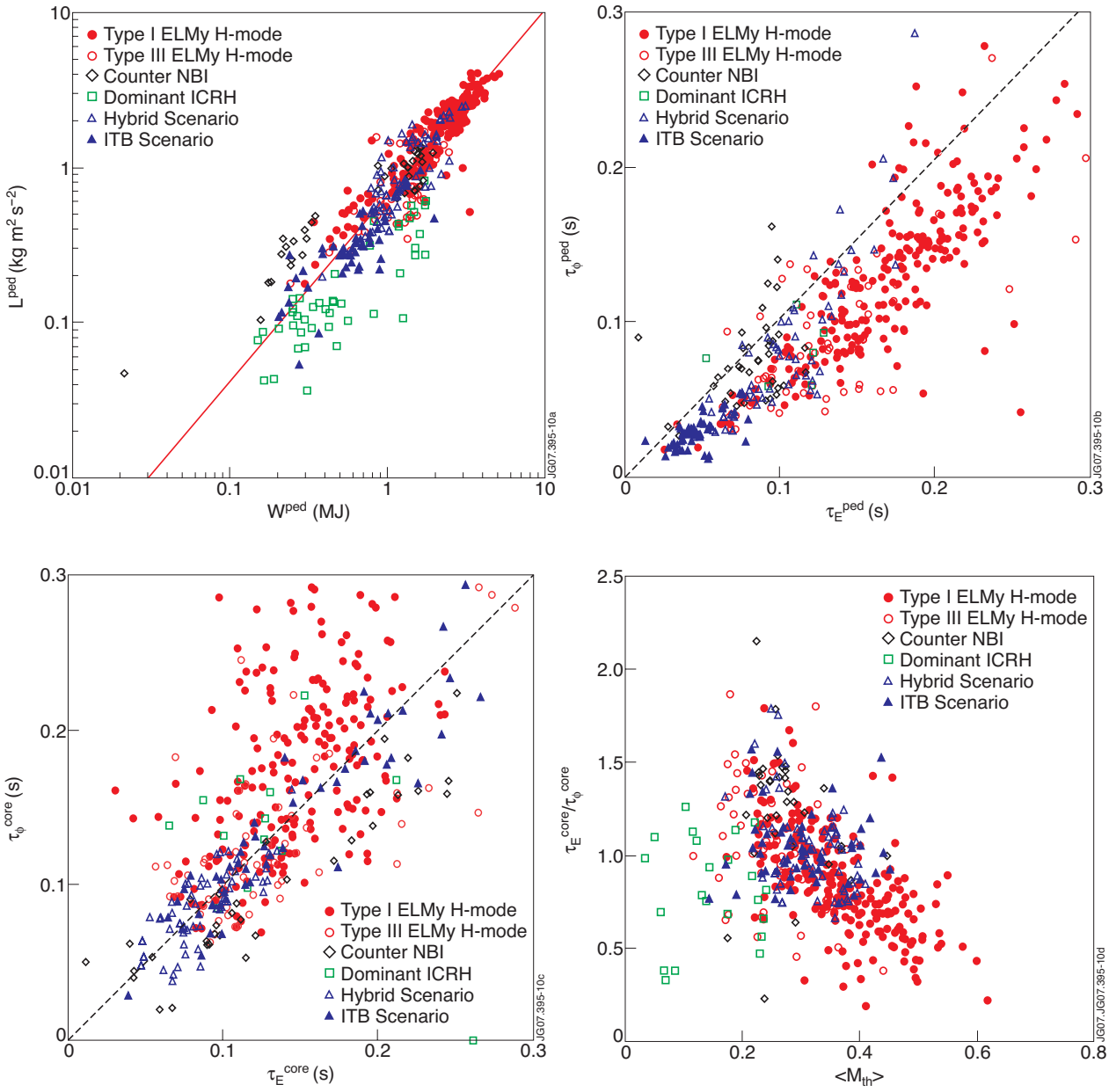

Figure 10: a) The pedestal (edge) momentum versus the pedestal energy. b) Comparison of the pedestal (edge) momentum and energy confinement times. c) Comparison of the core momentum and energy confinement times. d) The ratio of the core energy and momentum confinement times as a function of the average thermal Mach number.